Energy Conversion and Management 268 (2022) 115990

Contents lists available at ScienceDirect

Energy Conversion and Management

journal homepage: www.elsevier.com/locate/enconman

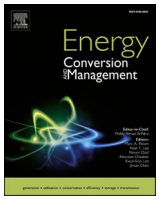

Optimization and performance analysis of water-mediated series indirect evaporative chillers: Experimental and simulated investigation

Yang Jing, Ce Zhao, Xiaoyun Xie *, Yi Jiang

Building Energy Research Center, Tsinghua University, Beijing 100084, People's Republic of China

ARTICLE INFO

Keywords:
Direct evaporative cooling
Dew point cooler
Water-mediated
Freezing
Flow rate

ABSTRACT

Evaporative cooling can be applied as a precooling or substitute technology for vapor compression refrigeration systems to save energy and reduce pollution emissions. This paper reports an experimental and numerical investigation of water-mediated series indirect evaporative chillers. An experimental unit was developed for the first time to produce cooling water for a hospital in Xinjiang Province, China. The wet-bulb efficiency of the cooling unit was measured to be above 106.57%, and the dew-point efficiency was 25.81–53.35%. The optimal air and water flow rates in the direct evaporative cooling process are approximately equal and independent of the heat and mass transfer coefficient of the padding. A case study shows that series indirect evaporative cooling is a more befitting process for 63.48% of Beijing's cooling season duration and 36.52% for direct evaporative cooling. The anti-freezing evaluation results show that series indirect evaporative cooling greatly reduces the risk of freezing in cold regions. The performance comparison and flow optimization studies in this paper can provide guidelines for the choice and design of evaporative cooling process. Water-mediated series indirect evaporative cooling performs better in dry and hot regions compared to direct evaporative cooling.

1. Introduction

Nowadays, the building sector accounts for one third of total energy consumption and 30% of total CO_2 (carbon dioxide) emissions in the end-use sector [1]. As global GDP (gross domestic product) grows and urbanization increases, energy consumption and CO_2 emissions in the building sector will continue to expand. One of the most important factors in the growth of energy consumption is the spread of HVAC (heating, ventilating, and air condition) systems and the growing demand for better indoor thermal comfort [2]. HVAC systems make up the vast majority of final energy use in the building sector (approximately 50% of building consumption and 20% of total consumption in the USA) [3].

It is thus important to seeking a more efficient refrigeration technology to replace the traditional vapor compression refrigeration to decrease energy consumption. Compared with the vapor compression refrigeration, evaporative cooling technology has some principal advantages, such as substantial energy and cost savings, life-cycle cost effectiveness, improved indoor air quality, reduced pollution emissions, and no use of chlorofluorocarbons [4]. Researchers have shown that evaporative cooling technology combined with a vapor compression system can significantly improve cooling system energy efficiency. Cui et al. [5] indicated a hybrid system, that combined indirect evaporative heat exchanger and a vapor compression system, was able to reduce 47% cooling load of the chiller for the outdoor humid air. Delfani et al. [6] introduced an indirect evaporative cooler as a pre-cooling unit for mechanical cooling system, which reduced about 75% cooling load and 55% electrical energy consumption of the mechanical cooling system. An almost 80% energy consumption reduction was obtained by using indirect evaporative cooling in fresh air conditioning applications [7]. Evaporative cooling can cover the entire cooling load in some dry regions. A two-stage evaporative cooling experimental setup was built in Iran with the wet-bulb effectiveness varied over a range of 108 to 111%, which could provide comfort condition in a vast region and save electric power input by 60% compared with mechanical vapor compression systems [8]. Fikri et al. [9] reported the experimental performance of a multistage direct–indirect evaporative cooler using a heat pipe in terms of saturation efficiency, the output air humidity, and sump water consumption.

Evaporative cooling can be classified into different categories, such as air-mediated vs water-mediated and DEC (direct evaporative cooling) vs IEC (indirect evaporative cooling) [10]; the indirect and air-mediated evaporative cooling has been more popular in recent years. DEC

* Corresponding author.
E-mail address: xiexiaoyun@tsinghua.edu.cn (X. Xie).

https://doi.org/10.1016/j.enconman.2022.115990
Received 10 February 2022; Received in revised form 7 July 2022; Accepted 8 July 2022
Available online 17 July 2022

Nomenclature

Symbols

A	transfer area (m^2)
c_{pa}	specific heat of air (kJ/(kg·K))
c_{pw}	specific heat of water (kJ/(kg·K))
COP	coefficient of performance
DEC	direct evaporative cooling
E	specific enthalpy (kJ/kg)
EER	energy efficiency ratio (-)
FCU	fan coil unit
G_a	inlet ambient air mass flow rate (kg/s)
G_w	inlet water mass flow rate (kg/s)
g	gravitational acceleration (m/s^2)
h	pump head (m)
$HVAC$	heating, ventilating and air condition
IEC	indirect evaporative cooling
KA	heat transfer coefficient (kW/ K)
k_d	mass transfer coefficient of padding ($kg/(m^2 \cdot s)$)
k_L	heat transfer coefficient of SHE ($kW/(m^2 \cdot K)$)
k_s	heat transfer coefficient of padding ($kW/(m^2 \cdot K)$)
P	pressure (Pa)
P_h	thermal pressure difference (Pa)
$\triangle P$	resistance (Pa)
Q	cooling capacity (kW)
r_0	latent heat of vaporization of water (kJ/kg)
RH	relative humidity (-)
S	flow coefficient (kg/m)
SHE	sensible heat exchanger
t	temperature (℃)
T	degree kelvin (K)
t_{ea}	temperature of wet air (℃)
v	air velocity (m/s)
W	power consumption (kW)
z	height difference

Greek symbols

ε	effectiveness
η	energy efficiency
ρ	density (kg/m^3)
ω	humidity ratio (g/kg dry air)

Subscripts

a	air
con	condenser
db	dry-bulb temperature
dp	dew-point temperature
eva	evaporator
in	inlet
int	internal
out	outlet
s	design condition
w	water
wb	wet-bulb temperature

researches mainly focused on investigating the heat and mass transfer performance of different padding materials, such as coconut coir, jute fiber and sackcloth [11]; date palm fibers, jute and luffa [12]; honeycomb and aspen cooling pad [13]; lithium- and bromine-enriched polyacrylamide hydrogels [14]; and PVC (polyvinyl chloride) sponge [15]. The research of indirect evaporative cooling mainly involves the development of different device structures and model optimization. The common IEC structures can be divided into classic [16], dew-point or regenerative [17], Maisotsenko cycle [18], multistage IEC [19] and desiccant arrangements [20].

Air-mediated evaporative cooling is usually applied in small-scale buildings like residential and commercial buildings. Harrouz et al. [21] used an integrated solar-windcatcher with a dew-point indirect evaporative cooler to meet the required thermal comfort and indoor air quality for classrooms. The rig can provide cold air with a temperature of 24.8 ℃ (±0.3℃), a relative humidity ranging between 43% and 58%, and a CO_2 level less than 900 ppm. An air-based Li-ion battery thermal management system was modified by integrating a direct evaporative cooling system by Zhao et al [22]. The experimental results showed that the DEC system with reciprocating air flow achieved a lower maximum temperature difference of 4.5 K. Horr et al. [23] investigated the experimental performance of an indirect evaporative cooling unit producing fresh air, which reduced 43% cooling capacity compared to dry operation. Pandelidis et al. [24] used a dew-point evaporative cooler to recover cooling capacity from indoor air to fresh air. The system can cover 95% of total cooling loads, significantly higher than a standard energy wheel which can cover only 9%. Air-mediated evaporative cooling systems occupy a large space, and it is difficult to achieve individual control over different demanded spaces [25]. Meanwhile, for buildings with large cooling loads or scattered users, fans of air-mediated cooling systems consume considerable power for long-distance transportation cooling capacity. Water-mediated indirect evaporative cooling has been widely applied in large-scale centralized cooling stations such as cooling towers, but few studies on water-mediated evaporative cooling are available. Yang et al. [10] reviewed recent literatures on evaporative cooling with water and air as working media, of which water-mediated IEC accounts for only a small proportion. Sipho and Tilahun [26] designed an indirect evaporative system to provide cooling water for the temporary storage of fruit and vegetables and reported a cooler efficiency of 88.04 to 95.6%. La et al. [27] proposed a novel rotary desiccant cooling system incorporating two-stage dehumidification and regenerative evaporative cooling to produce cooling water with a thermal coefficient of 0.3 to 0.6. Jiang and Xie [28] introduced a parallel indirect evaporative chiller in Xinjiang Province, China, which saved more than 40% electricity input compared with the traditional air conditioning system.

To fill the research gap in evaporative cooling, this study develops and tests the performance of a novel water-mediated series indirect evaporative chiller using returning cooling water to cool the ambient air. An experimental rig of a water-mediated series indirect evaporative chiller was developed in a hospital in the Akesu area, Xinjiang Province, China. A numerical model of the unit was developed and used for guiding the selection of optimal water and air flow rates of the padding. A comparison of the cooling performance under different water flow distribution and under different climatic conditions of DEC to series IEC helps engineers choose the appropriate water-mediated evaporative cooling process for different systems and meteorological conditions.

2. System description

The cores of water-mediated series indirect evaporative chillers are one (or more than one) SHEs (sensible heat exchanger) and a direct evaporative cooler (padding), as shown schematically in Fig. 1(a). Inlet cooling water (State D) first enters the sensible heat exchanger, where it cools the fresh, dry, and hot inlet air (State O). As a consequence, the fresh air wet-bulb temperature is markedly reduced (State A), and the cooling water is heated (Sate E), which is beneficial to the transfer process of padding [29]. The water leaving the sensible heat exchanger is sent to the top of the padding and sprayed. The cooling water contacts directly with dry air in the padding and is cooled (State F) to nearly the

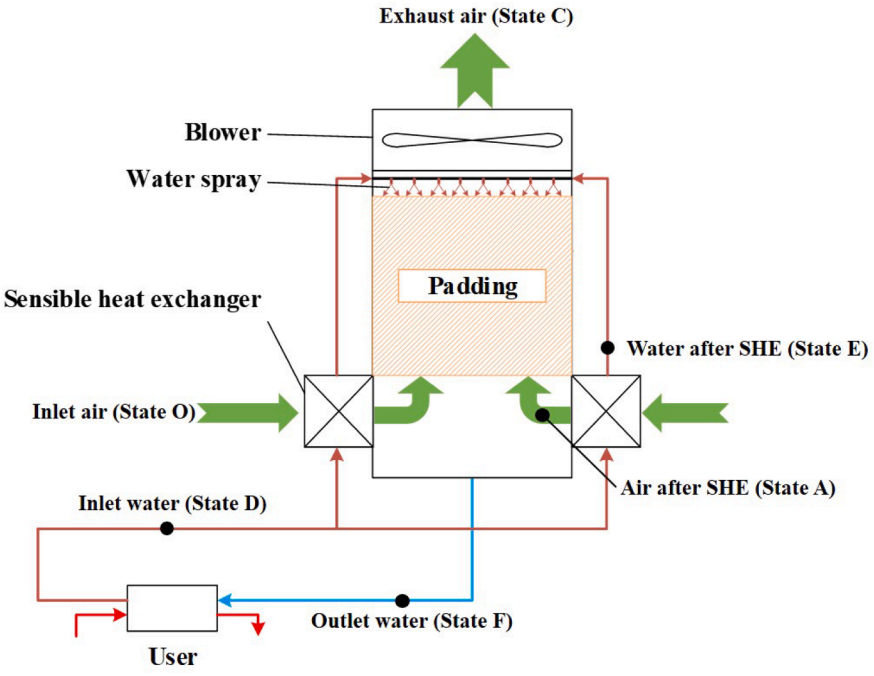

(a)

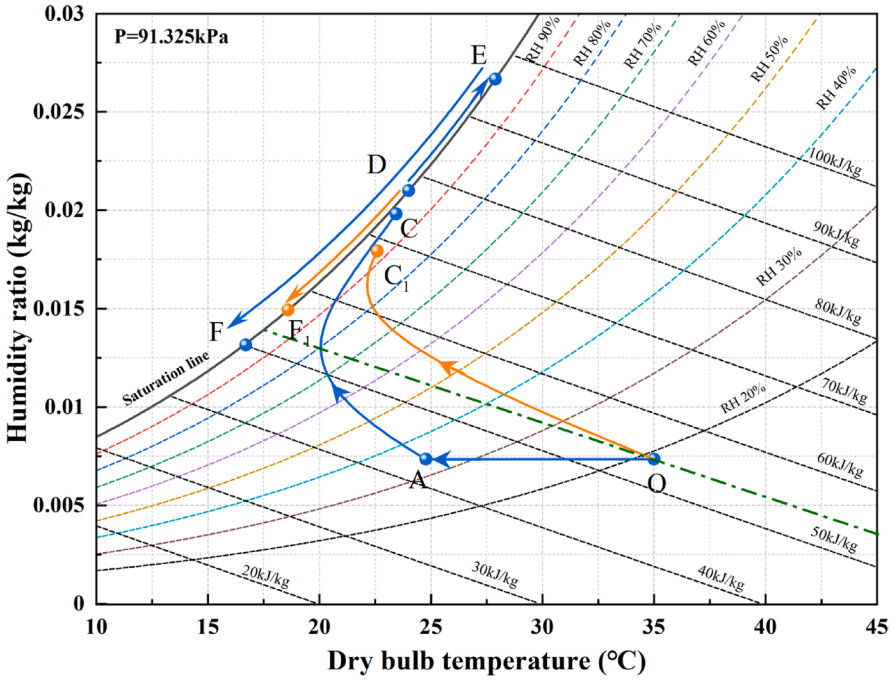

(b)

Fig. 1. Schematic of water-mediated series indirect evaporative chillers: (a) chiller structure; (b) cooling process on the psychrometric chart compared with DEC.

dew-point temperature of inlet air. This chiller can independently produce high-temperature cooling water, which can be applied as an energy-saving substitute for vapor compression chillers in hot and dry regions and as a precooling device to improve energy efficiency. Fig. 1 (b) shows the cooling process of the water-mediated series IEC and DEC on the psychrometric chart. The sensible heat exchanger reduces inlet air dry and wet bulb temperature and improves the heat and mass transferability of padding, making series IEC's wet-bulb efficiency significantly higher than DEC's and even greater than 100%.

3. Experimental setup and mathematical model

In this part, the detailed design parameters of experimental setup and the measurement system are presented, and the assumptions and calculation principles of the numerical model are introduced.

3.1. Experimental rig

To investigate the thermodynamic performance of water-mediated series indirect evaporative chillers, an experimental rig with a design cooling capacity of 500 kW was built in the Akesu area, Xinjiang Province, China, as shown in Fig. 2. The whole experimental unit includes 4 × 2 sensible heat exchangers, padding, pump, FCU (fans and fan coil units). Each sensible heat exchanger has 12 rows of copper tubes, and aluminum fins are used on the surface of copper tubes to enhance heat transfer. The size of the air inlet of the sensible heat exchanger is 1.4 × 1.52 m^2, and the total heat transfer area of the heat exchanger is 526 m^2. The material of the padding is corrugated papers, and the size of which is 6 × 4 × 3.5 m^3 (*length* × *width* × *height*). The sensible heat exchangers recover cooling capacity from returned cooling water to pre-cool ambient air. The corrugated paper padding increases the contact area between air and water and improves the heat and mass transfer rate. The air flow rate is controlled by six Frequency-controlled fans with a nominal flow rate of 31000 m^3/h, and the water flow rate is set at 120 m^3/h controlled by the pump. The supplied cooling water provides cooling for end users in FCUs.

The parameters to be measured include the air flow rate, water flow rate, air dry temperature, air relative humidity, water temperature, air pressure difference, and electric power. The measurement instrument and accuracy for each parameter are shown in Table 1.

3.2. Model development

With the temperature and humidity of the inlet air as the main variables, which can be varied to simulate the system performance on different installation locations. The model includes a two-dimensional semi-counter flow sensible heat transfer sub-model and a one-dimensional counterflow heat and mass transfer sub-model (padding). The following assumptions are adopted:

(1) No heat losses to the surroundings.
(2) Uniform air inlet conditions [30] and spray water film [31].
(3) The advection term is dominant, and the diffusion term is negligible [32].
(4) The constant Lewis's number is equal to 1.
(5) Uniform thermos-physical properties of the air and water within each control volume, while the fluid properties are considered constant [32].

The finite difference method was adopted to build this series indirect evaporative cooling model. Sensible heat exchangers and padding are divided into several small control volumes, and the internal temperature and humidity within each difference are uniform. Fig. 3 shows the model governing equations of the water-mediated series indirect evaporative cooling model. Within each control volume of the discretized SHE, the air and water exchanges heat in a semi-counter flow condition.

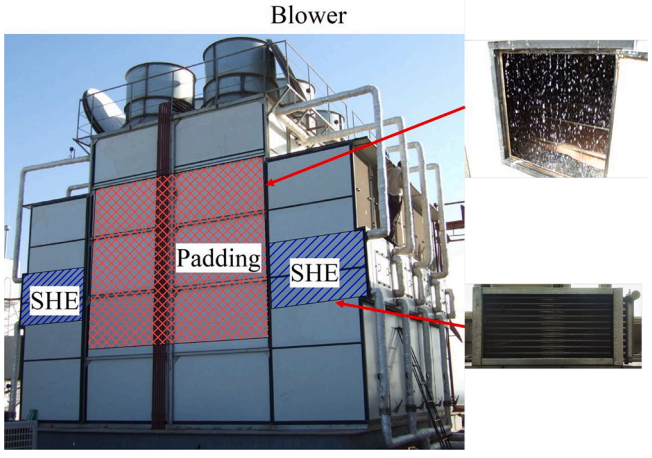

Fig. 2. The developed water-mediated series indirect evaporative chiller.

Table 1
Specification of various measuring instruments.

Parameters	Symbol	Instrument	Accuracy
Air dry temperature (℃)	$t_{a,db}$	Electronic precision long-time thermo-Hygrograph	±0.5℃
Air relative humidity (-)	RH	Electronic precision long-time thermo-Hygrograph	±3%
Water temperature (℃)	t_w	Thermocouple thermometer	±0.3℃
Air velocity (m/s)	v	Thermal anemometer ball	±2%
Water flow rate (m^3/s)	G_w	Ultrasonic flowmeter	±5%
Air pressure difference (mm)	ΔP	Pitot tube and micromanometer	±0.2%
Electric power (kW)	W	Power meter	±0.1%

$$G_a \cdot c_{pa} \cdot dt_a = -k_L \cdot dA \cdot (t_a - t_w) \tag{1}$$

$$G_a \cdot c_{pa} \cdot dt_a = -G_w \cdot c_{pw} \cdot dt_w \tag{2}$$

$$\frac{G_a}{k} \cdot c_{pa} \cdot (t_a[i,j-1] - t_a[i,j]) = -\frac{k_L A_{SHE}}{12k} \cdot (t_a[i,j] - t_w[i,j]) \tag{3}$$

$$\frac{G_a}{k} \cdot c_{pa} \cdot (t_a[i,j-1] - t_a[i,j]) = \begin{cases} G_w \cdot c_{pw} \cdot (t_w[i,j] - t_w[i-1,j]) \text{ (j is odd number)} \\ (i=0,k), (j=0,12) \\ G_w \cdot c_{pw} \cdot (t_w[i-1,j] - t_w[i,j]) \text{ (j is even number)} \end{cases} \tag{4}$$

$$Q_{SHE} = G_w \cdot c_{pw} \cdot (t_w[0,12] - t_w[0,0]) \tag{5}$$

$$t_w[0,0] = t_{w,in} \tag{6}$$

$$t_a[0,i] = t_{a,in,db} (i = 0,k) \tag{7}$$

$$\begin{cases} t_w[k,j] = t_w[k,j+1] \text{ (j is odd number)} \\ j = 1, 11 \\ t_w[0,j] = t_w[0,j+1] \text{ (j is even number)} \end{cases} \tag{8}$$

$$t_{a,SHE,out} = \frac{\sum_{i=1}^{k} t_a[i,12]}{k} \tag{9}$$

$$t_w[0,12] = t_{w,SHE,out} \tag{10}$$

$$\omega_{a,SHE,out} = \omega_{a,in} \tag{11}$$

where G_a and G_w represent the air and water mass flow rates, respectively, and k_L is the sensible heat transfer coefficient of air and water in SHE. c_{pa} and c_{pw} represent the constant pressure-specific heat of air and water. $t_{w,in}$ is the returned cooling water temperature, and $t_{a,in,db}$ is the inlet ambient air dry-bulb temperature.

Equation (3) expresses the air to water sensible heat transfer process, and equation (4) is the energy conservation. Equations (6) and (7) are the inlet temperature of water and air, which is also the initial and boundary condition of this model. Equations (9) ~ (11) is the air and water temperature and humidity output of the SHE sub-model.

A direct evaporative cooling process occurs in the padding, which can be simplified to a 1-dimensional counterflow heat and mass transfer model. Water is sprayed on the top of the padding and contacts air directly in the padding, transferring heat and part of the moisture from the water to the dry air. The theoretical formula of this process is as follows [28]:

$$G_a \cdot c_{pa} \cdot dt_a = -k_s \cdot dA \cdot (t_w - t_a) \tag{12}$$

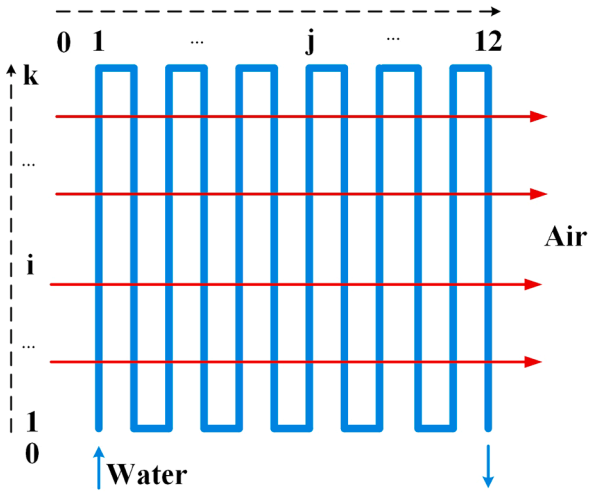

(a) Two-dimensional semi-counter flow sensible heat exchangers model

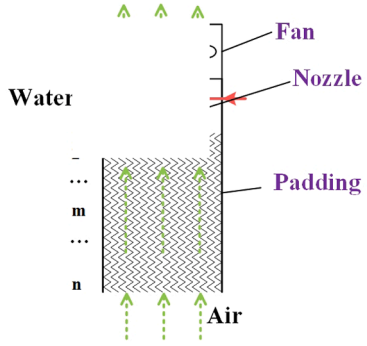

(b) One-dimensional counterflow padding model

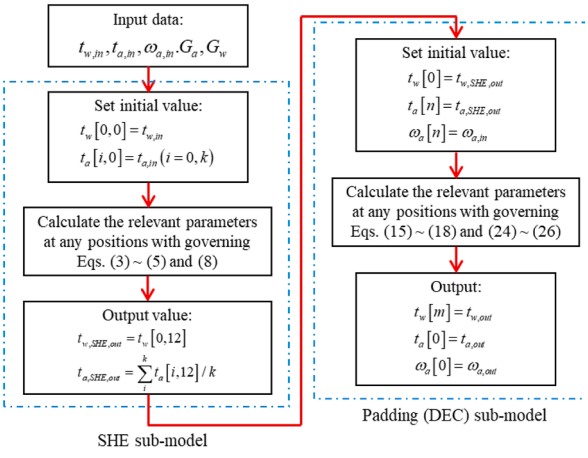

(c) Calculation flow chart of the simulated model.

Fig. 3. Principle of water-mediated series IEC model.

$$G_a \cdot d\omega_a = -k_d \cdot dA \cdot (\omega_w - \omega_a) \tag{13}$$

$$G_w \cdot c_{pw} \cdot dt_w = k_s \cdot dA \cdot (t_a - t_w) + r_0 \cdot k_d \cdot dA \cdot (\omega_a - \omega_w) \tag{14}$$

$$G_a \cdot c_{pa} \cdot (t_a[m-1] - t_a[m]) = \frac{k_s A_{padding}}{n} \frac{(t_w[m-1] - t_a[m-1]) + (t_w[m] - t_a[m])}{2} \tag{15}$$

$$G_a \cdot (\omega_a[m-1] - \omega_a[m]) = \frac{k_d A_{padding}}{n} \frac{(\omega_w[m-1] - \omega_a[m-1]) + (\omega_w[m] - \omega_a[m])}{2} \tag{16}$$

$$G_w \cdot c_{pw} \cdot (t_w[m-1] - t_w[m]) = \frac{k_s A_{padding}}{n} (E_{wa}[m] - E_a[m]) \tag{17}$$

$$G_a \cdot (E_a[m-1] - E_a[m]) = \frac{k_s A_{padding}}{n} (E_{wa}[m] - E_a[m]) \tag{18}$$

$$Q_{padding} = G_w \cdot c_{pw} \cdot (t_w[0] - t_w[n]) \tag{19}$$

$$Lewis = \frac{k_s}{c_{pa} \cdot k_d} \approx 1 \tag{20}$$

$$t_w[0] = t_{w,SHE,out} \tag{21}$$

$$t_a[n] = t_{a,SHE,out} \tag{22}$$

$$\omega_a[n] = \omega_{a,SHE,out} \tag{23}$$

$$E_a[m] = Enthalpy(AirH_2O, T = t_a[m], \omega = \omega_a[m], P = P_0) \tag{24}$$

$$E_{wa}[m] = Enthalpy(AirH_2O, T = t_w[m], RH = 100\%, P = P_0) \tag{25}$$

$$\omega_w[m] = Humidity(AirH_2O, T = t_w[m], RH = 100\%, P = P_0) \tag{26}$$

$$t_{w,out} = t_w[m] \tag{27}$$

$$t_{a,out} = t_a[0] \tag{28}$$

$$\omega_{a,out} = \omega_a[0] \tag{29}$$

where k_s and k_d represent the sensible heat and mass transfer coefficient of air and water, respectively. r_0 represents latent heat for the vaporization of water. ω_a and ω_w represent the humidity ratio of air and equivalent humidity ratio of water, respectively. E_a and E_{wa} are the enthalpy of air and water, and ω_w represent the humidity of saturated wet air on the cooling water surface. Equations (21) ~ (23) are the initial condition of this padding model, and equations (27) ~ (29) are the simulated results.

Fig. 3(c) shows the calculation flow chart of this model, which consists of a SHE sub-model and a padding sub-model. The padding sub-model is essentially a direct evaporative cooling process. The input conditions include inlet ambient air temperature, humidity and flow rate, and returned cooling water flow rate and temperature. The initial conditions are firstly input into the SHE sub-model to calculate the sensible heat transfer process of air precooling and to obtain the intermediate parameters of water and air. Then the intermediate parameters are used to simulate the counterflow heat and mass transfer process to get the final results of supplying water temperature.

4. Experimental results and model verification

The experimental performance at different ambient air conditions and inlet water conditions are studied, and this section also validates the numerical model using the experimental test data.

4.1. Experimental results

The experimental results of air flow rate and pressure difference can be measured directly, as shown in Table 2 and Table 3. The measured position was in the air inlet of the sensible heat exchanger, located in the south and north sides of the experimental setup, and each side has 4 sensible heat exchangers. The average ambient air velocities on the south and north side were 2.269 m/s and 2.125 m/s respectively, and the corresponding air volume flow rates were 73018 m^3/h and 68392 m^3/h. The operating total air flow rate was 141410 m^3/h and remained basically constant during experiment. Pitot tube and micromanometer were used to measure resistance of sensible heat exchangers and padding. The pressure difference between air outlet of SHE and ambient air was 167.07 Pa, and the pressure difference between air outlet of padding and ambient air was 294.94 Pa. The pressure drops of sensible heat exchangers and padding were 167.07 Pa and 127.87 Pa. The power consumption of pump and fans is shown in Table 4, and the total power consumption was 57.80 kW.

The following performance indicators are used to evaluate the performance of the series IEC chillers: wet-bulb efficiency, dew-point efficiency, cooling capacity, and EER (energy efficiency ratio), which are expressed in equations (1) ~ (4). The wet-bulb and dew-point efficiency reflect the overall performance of the equipment, and the SHE and padding efficiency reflect the performance of each component.

$$\varepsilon_{wb} = \frac{t_{water,in} - t_{water,out}}{t_{water,in} - t_{air,in,wb}} \tag{30}$$

$$\varepsilon_{dp} = \frac{t_{water,in} - t_{water,out}}{t_{water,in} - t_{air,in,dp}} \tag{31}$$

$$Q = G_w c_{pw}\left(t_{w,in} - t_{w,out}\right) \tag{32}$$

$$EER_{IEC} = \frac{Q}{W_{pump} + W_{fan}} \tag{33}$$

The experimental performance of indirect evaporative chillers was given under different inlet water and air conditions in this section. The outlet water temperature (State F), cooling capacity, and dew-point efficiency reflect the equipment performance at the same designed parameters. The following equation was used for uncertainty analysis of the experiment, taking the cooling capacity as an example:

$$\Delta Q\left(t_{w,in}, t_{w,out}, G_w\right) = c_{pw}\sqrt{\left(\Delta G_w\left(t_{w,in} - t_{w,out}\right)\right)^2 + \left(G_w \Delta t_{w,in}\right)^2 + \left(G_w \Delta t_{w,out}\right)^2} \tag{34}$$

Fig. 4(a) presents the relationship between the chiller outlet water temperature and meteorological conditions. The degree of correlation with outlet water temperature is dew-point, wet-bulb, and dry-bulb temperature in descending order, while the order of direct evaporative coolers is wet-bulb, dry-bulb, and dew-point temperature. The outlet water temperature is between the wet-bulb temperature and the dew-point temperature, indicating that its wet-bulb efficiency is greater than 100%. Fig. 4(b) shows that the cooling capacity and dew-point efficiency vary from 205.37 kW to 364.48 kW and 31.78% to 36.27%, respectively, as the operating water flow rate changes. The heat and mass transfer coefficients of padding and sensible heat exchangers can be calculated by taking inlet and outlet experimental results into the simulation model. The sensible heat coefficient of SHE is 30.93 kW/K/m^2, and the heat and mass transfer coefficients are 1.66 kW/K/m^3 and 1.65 kg/s/m^3, respectively.

Table 2
Experimental results of air flow rate.

Measuring position	Air outlet of SHE			
Air velocity (South) (Unit: m/s)			Air velocity (North)(Unit: m/s)	
Measure point 1	2.07	2.19	Measure point 1	2.13
Measure point 2	2.37	2.34	Measure point 2	2.15
Measure point 3	2.29	2.29	Measure point 3	2.14
Measure point 4	2.32	2.28	Measure point 4	2.08
Average(m/s)	2.269		Average (m/s)	2.125
South (m^3/h)	73,018		North (m^3/h)	68,392
Total (m^3/h)	141,410			

Table 3
Experimental results of pressure.

Measuring position (Unit: mm)		Air outlet of SHE			
Height difference	Measure point 1	Measure point 2	Average	Scale	Pressure (Pa)
South	55	54.8	53.275	0.4	−167.07
North	52	51.3			
Measuring position (Unit: mm)		Air outlet of padding			
Height difference	Measure point 1	Measure point 2	Average	Scale	Pressure (Pa)
South	97.5	94	94.05	0.4	−294.94
North	89.4	95.3			
Pressure difference of SHE	167.07 Pa	Pressure difference of padding		127.87 Pa	

Table 4
Experimental results of pump and fans power consumption.

Component	Power (kW)
Pump	16.66
Fan 1	6.93
Fan 2	6.96
Fan 3	7.03
Fan 4	6.76
Fan 5	6.74
Fan 6	6.72
Total	57.80

The mass flow ratio of air and water was 1.55–1.7, and the temperature difference of cooling water ranged from 1.43 K to 4.71 K with an average of 2.42 K. In this set of experimental results, the dew-point efficiency was stable, and the cooling capacity increased with decreasing inlet air dew-point temperature, which was due to the relatively high mass flow ratio of air and water. The EER of the indirect evaporative cooling system was calculated to be in the range of 3.55 to 6.31, and the average EER is 5.25. The lower temperature difference of cooling water leaded to high energy consumption of pump and fans, resulting in low EER of the experimental unit.

Fig. 4 indicates that the dew-point temperature has the greatest influence on indirect evaporative chillers. The variations in cooling capacity and dew-point efficiency with inlet air dew-point temperature are shown in Fig. 5. The cooling capacity and dew-point efficiency generally decrease with increasing dew-point temperature except for the first group of experimental data marked by the left side of the diagram, and their variation ranges are 194.85–350.67 kW and 36.28–53.35%, respectively.

The experimental rig can be used to produce cooling water lower than the inlet wet-bulb temperature, and thus its performance is obviously better than that of the direct evaporative cooler in hot and dry regions. The water-mediated series indirect evaporative chiller was observed to have a wet-bulb efficiency of over 106.57%, a cooling capacity of 134.28–566.45 kW, an EER of 3.55–6.31 and a dew-point efficiency of 25.81–53.35% under different operating conditions.

4.2. Model verification

The developed mathematical model was verified by the measured data. First, a group of data (shown in Table 5) were randomly selected to calculate the sensible heat coefficient of SHE and heat and mass transfer

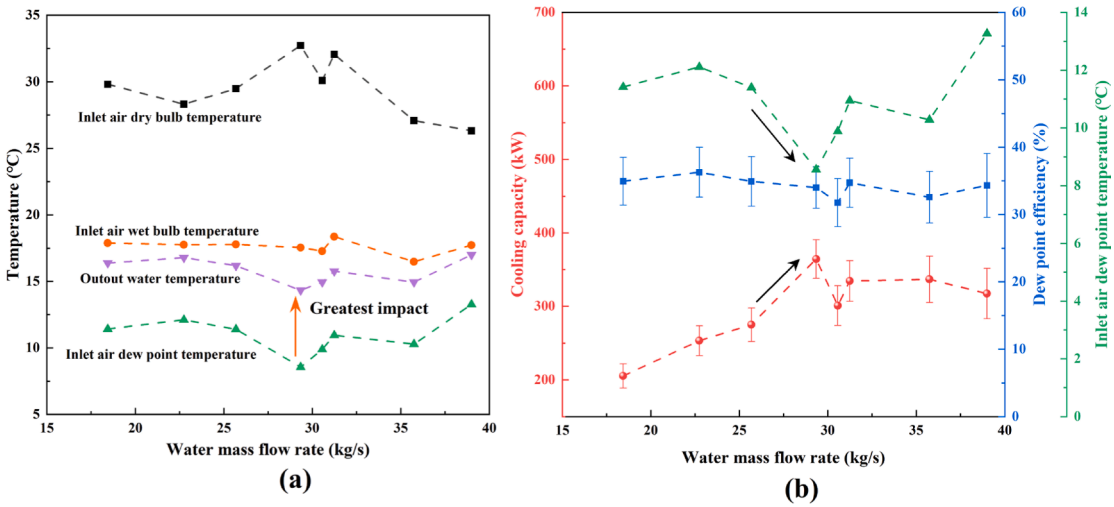

Fig. 4. Experimental results versus water mass flow rate; (a) inlet air conditions and output water temperature; (b) cooling capacity and dew-point efficiency.

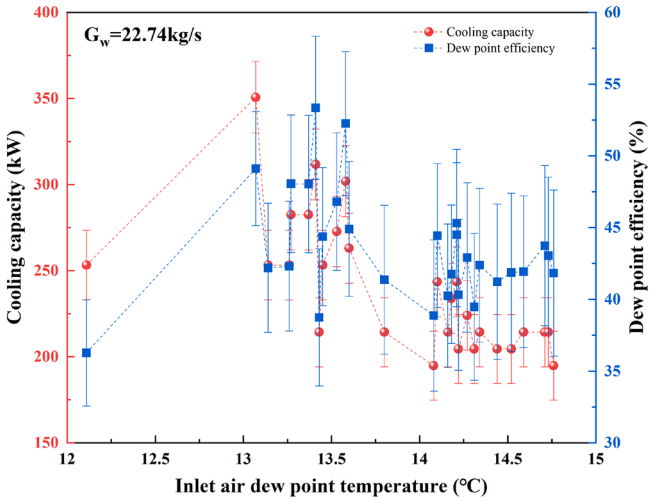

Fig. 5. Cooling capacity and dew-point efficiency versus inlet dew-point temperature.

Table 5
Parameters of experimental data.

Parameter	Symbol	Unit	Value
Water mass flow rate	G_w	kg/s	22.74
Air flow rate	G_a	m^3/h	141,410
Inlet air dry-bulb temperature	$t_{air,in,db}$	℃	27.08
Inlet air wet-bulb temperature	$t_{air,in,wb}$	℃	18.04
Inlet water temperature	$t_{water,in}$	℃	19.56
Outlet water temperature	$t_{water,out}$	℃	16.28
Water temperature after SHE	$t_{water,out,SHE}$	℃	23.62
Air dry-bulb temperature after SHE	$t_{air,out,db,SHE}$	℃	20.68

coefficients of padding by using the model. The sensible heat coefficient of SHE is 30.93 kW/K/m^2, and the heat and mass transfer coefficients of padding are 1.66 kW/K/m^3 and 1.65 kg/s/m^3, respectively. This shows that the Lewis number assumed in this cooling process is approximately equal to 1 is realistic. It is assumed that the heat and mass transfer coefficients of SHE and padding are constant during the model verification process.

Fig. 6 shows the model validation of continuous measurement experimental data under constant air and water flow rates. Fig. 6(a) displays the change in inlet air dry-bulb, inlet air wet-bulb, and inlet water temperature versus time, and the inlet air conditions can be represented in the psychrometric chart in Fig. 6(d). Fig. 6(b) shows the comparison between the experimental and simulated results of the output parameters. Fig. 6(c) reflects the relative error of the output parameters, most of which are within 5%. Moreover, the simulated results of output temperature are basically smaller than the experimental results, indicating that under this operating condition, the set transfer coefficient of SHE and padding is rather large.

Fig. 6 verifies the accuracy under the water flow rate condition of 22.74 kg/s, and Fig. 7 indicates the difference between the simulated and experimental results versus different water mass flow rates. The relative error of the majority of simulated points in Fig. 7 (a) is within 5% and the maximum error is 6.61%, reflecting the high accuracy of the established model. In summary, Fig. 6 and Fig. 7 show that the simulated results are in good agreement with the experimental results, and the established mathematical model has high accuracy.

5. Results and discussion

In this part, the optimization of air and water flow rate, comparison of system performance between DEC and series IEC for different climatic conditions and the anti-freezing performance of water-mediated series IEC are introduced by using proven model.

5.1. Optimization of padding air and water flow rate

The factors effecting EER of evaporative cooling mainly include pump and water energy consumption. Pump energy consumption is affected by the size of the cooling system, such as building height and cooling capacity. Evaporative cooling fan power consumption is determined by the resistance characteristics of the padding and sensible heat exchanger and air flow rate. When the heat and mass transfer coefficients of the padding and sensible heat exchanger increase, the output water temperature decreases, but the initial investment increases. Variations in air flow rate affect both fan energy consumption and output water temperature, which are reflected in system EER.

The influence of the air and water flow rates on the evaporative cooling performance has been investigated in many previous studies, but the optimal flow rates are still not clearly given. A widely accepted rule is that at the same cooling water flow rate, a larger air flow rate causes better thermal performance of direct evaporative coolers. However, larger air and water flow rates require more pump and fan power consumption, which result in a lower EER of the whole cooling system. Reducing air and water flow rates could result in lower cooling capacity or higher producing water temperature of evaporative cooling, causing

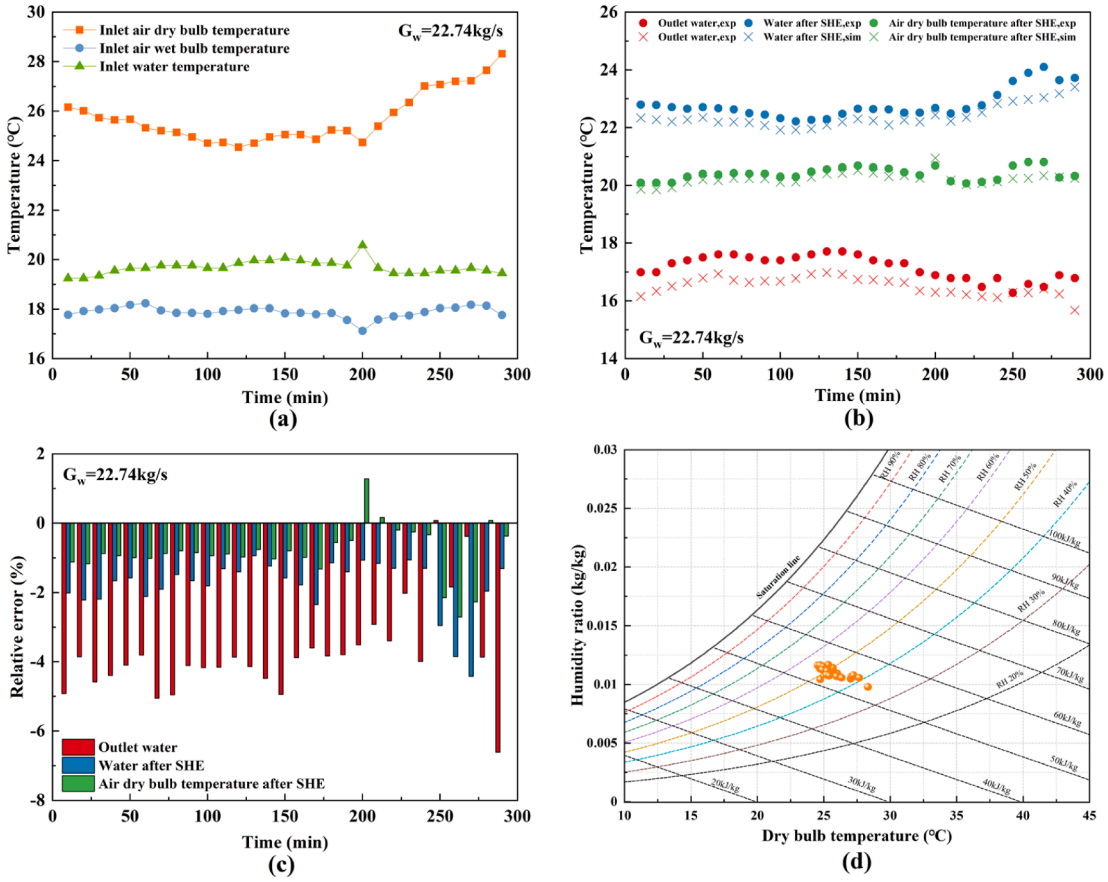

Fig. 6. Comparison between experimental and simulated results; (a) inlet air and water temperature; (b) output results; (c) relative error; (d) inlet air parameters shown on the psychrometric chart.

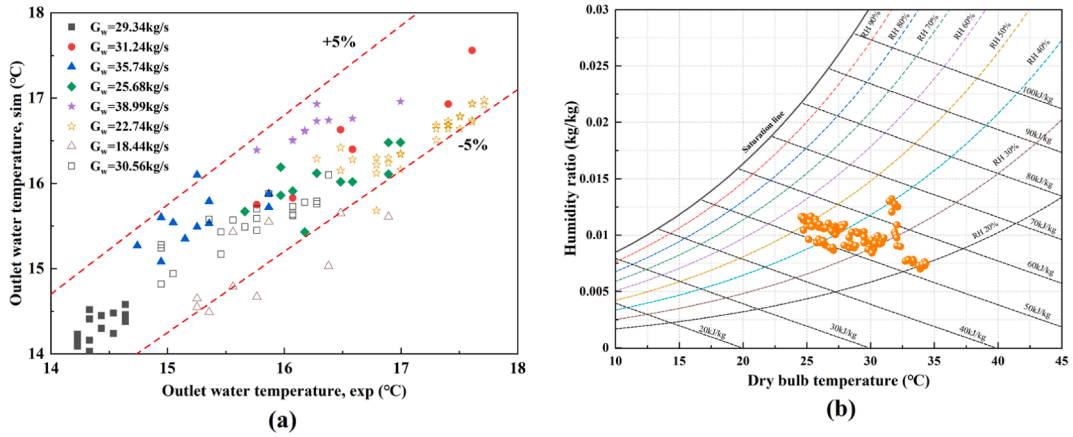

Fig. 7. Comparison of outlet water temperature under different water flow rates; (a) relative error; (b) inlet air parameters shown on the psychrometric chart.

the increased electrical consumption of the mechanical vapor compression chiller. The increase of heat and mass transfer area improves the system EER but also increases the initial investment.

As the two parameters counter each other, it is thus an important research question to design an evaluation method that can weigh these two parameters equally as attributors to the system performance and identify an optimal operating condition which can bring the entire system to a highest EER. A simple traditional cooling system using an evaporative cooler was built to take this problem into account, as shown in Fig. 8(a). The decrease in the water output temperature of evaporative cooling reflects that the condensing temperature of vapor compression refrigerators can be reduced and the electrical efficiency can be improved. To evaluate the whole system's performance, the energy efficiency ratio (EER) is adopted under different air and water conditions.

$$EER = \frac{Q}{W + W_{pump} + W_{fan}} \tag{35}$$

$$COP = \frac{Q}{W} = \frac{T_{eva}}{T_{con} - T_{eva}}\eta \tag{36}$$

$$W_{pump} = \frac{G_w \cdot g \cdot h}{\eta_{pump}} \tag{37}$$

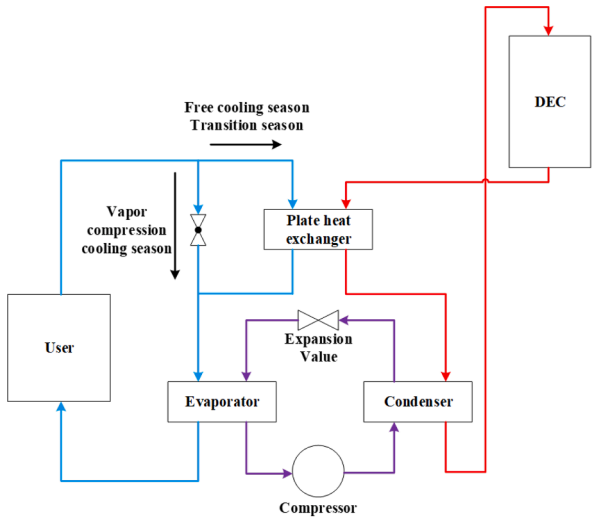

(a) Case 1: DEC system.

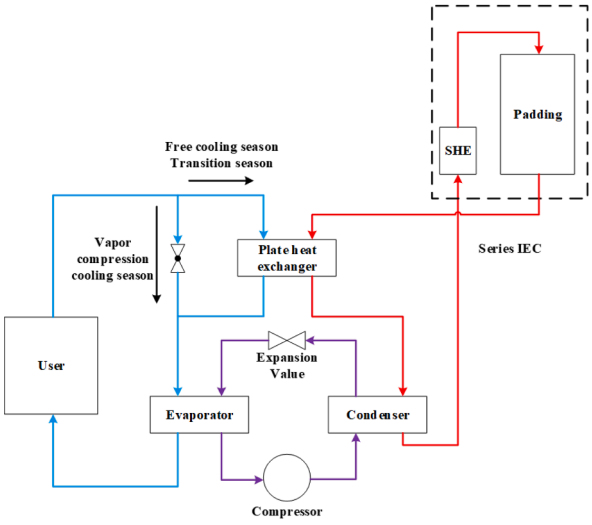

(b) Case 2: series IEC system.

Fig. 8. Traditional DEC and series IEC cooling system; (a) DEC system; (b) series IEC system.

$$W_{fan} = \frac{G_a \cdot \Delta P}{\rho_{air} \cdot \eta_{fan}} \tag{38}$$

where Q represents the cooling load, W is the power consumption of vapor compression chillers; W_{pump} and W_{fan} represent the power consumption of pumps and fans, respectively. η is the thermodynamic efficiency of vapor compression refrigerators, and η_{pump} and η_{fan} represent the energy efficiency of pumps and fans.

The main parameters affecting the system EER of the direct evaporative cooling include water flow rate, air flow rate and padding heat and mass transfer coefficient. Better padding performance causes higher initial investment; however, its effect on system performance is not discussed in this paper. With the same cooling capacity and required cooling water temperature, the lower water flow rate means lower pump energy consumption but higher energy consumption of the mechanical vapor compression chiller. Lowering the air flow rate of evaporative cooling can reduce the energy consumption of the fan, but at a cost of bringing the system to work at a higher supplied cooling water temperature and a higher mechanical vapor compression chiller energy consumption. So proper water and air flow rates result in higher EER and thermal comfort for the evaporative cooling system.

First, the effects of air and water flow rates on the direct evaporative cooling performance at system level are studied. For the system in Case 1, the air and water flow rates were optimized, while the relevant parameter settings are shown in Table 6, and the results are shown in Fig. 9. The system setting parameters refer to the actual experimental data of the developed water-mediated series evaporative cooling system. The EER increases first and then decreases slowly with both the air and water flow rates, and there is an optimal air and water flow rate in the set system. Possible influencing factors include cooling capacity, heat and mass transfer coefficient, outdoor meteorological conditions, and so on.

In the design process of a cooling system, it is a rule of thumb to choose the appropriate refrigeration equipment based on its cooling load. Thus, the optimal performance and flow rate of the system at different *KA* (heat transfer coefficient) are studied in Fig. 10. As *KA* increases, the largest EER increases, but so does the corresponding initial investment. The optimal flow rates remain unchanged, which indicates that it has nothing to do with *KA* and cooling load. On this basis, the optimal flow rate can be theoretically calculated by assuming that *KA* is infinite and that outlet parameters satisfy the following relations:

$$t_{water,out} = t_{air,in,wb} \tag{39}$$

$$t_{air,out,db} = t_{air,out,wb} = t_{water,in} \tag{40}$$

Therefore, for the *KA* of padding to be infinite, the output of evaporative cooling must satisfy at least one of the equations (39) or (40). When the conditions given by equation (39) are met, the cooling water flow rate, returned temperature, supplied temperature, inlet ambient air conditions and other parameters remain unchanged, and system EER can be expressed in equation (41). Since the supplied water temperature of evaporative cooling is the same as the ambient air wet-bulb temperature, and the water flow rate is unchanged, the energy consumptions of the mechanical vapor compression chiller and pump are constant. At this point, system EER is only related to the inlet air flow rate, and the lower air flow rate leads to the higher system EER. The minimum inlet air flow rate G_a under the condition shown in equation (39) is equation (42).

$$EER = \frac{Q}{W + W_{pump} + W_{fan}} = \frac{G_w \cdot c_{pw}\left(t_{w,in} - t_{w,out}\right)}{W + \frac{G_w \cdot g \cdot h}{\eta_{pump}} + \frac{G_a \cdot \Delta P}{\rho_{air} \cdot \eta_{fan}}} \tag{41}$$

$$G_a = \frac{G_w \cdot c_{pw}\left(t_{w,in} - t_{a,in,wb}\right)}{\left(E_{w,in} - E_{a,in}\right)} \tag{42}$$

The ideal optimal flow rate ratio of air and water was calculated by considering Eq. (42) under different inlet air conditions, as shown in Fig. 11. The optimal mass flow rate ratio is close to 1, and the air flow rate needs to increase as the humidity increases. The main reasons behind different ideal optimal flow ratios are twofold. First, the air saturation line of the psychrometric chart is nonlinear, while the enthalpy of water is approximately linear with temperature. Second, at

Table 6
System setting parameters.

Parameter	Symbol	Unit	Value
Thermodynamical efficiency	η	–	0.6
Pump energy efficiency	η_1	–	0.7
Fan energy efficiency	η_2	–	0.7
Pump head of case 1	h	m	35
Fan total pressure of case 1	ΔP	Pa	200
Pump head of case 2	h	m	40
Fan total pressure of case 2	ΔP	Pa	300

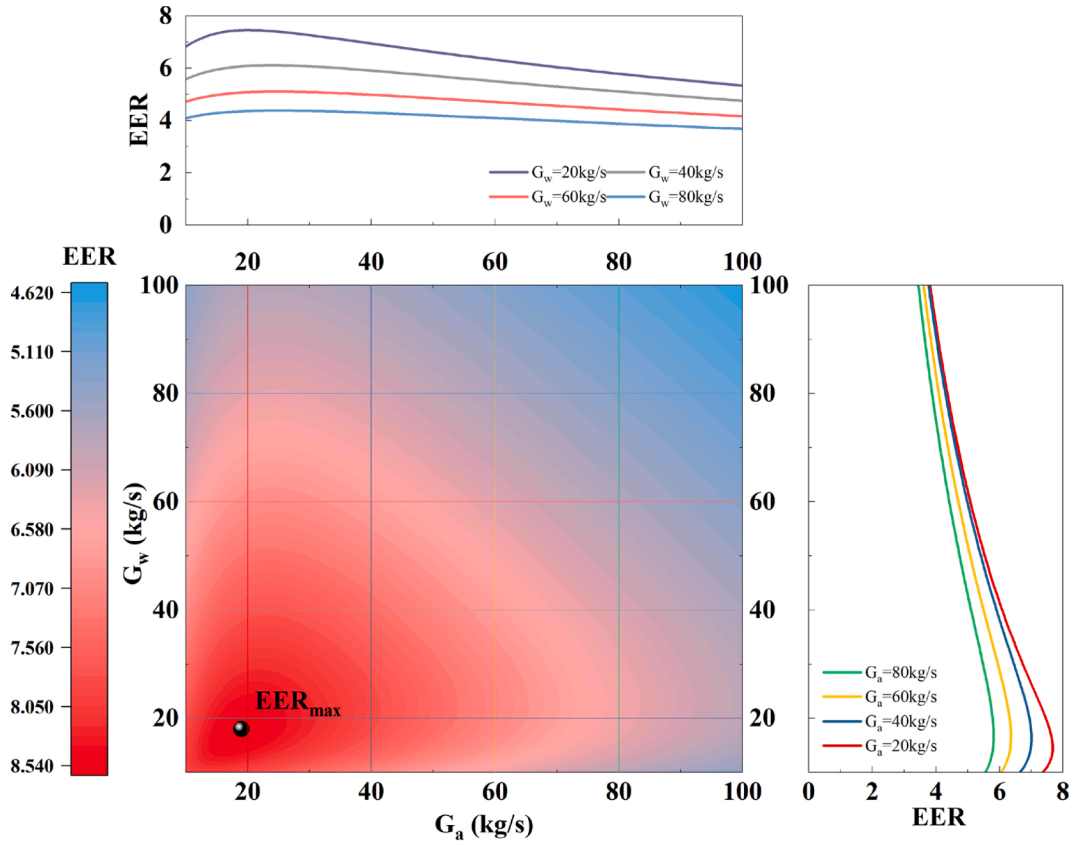

Fig. 9. System EER under different air and water mass flow rates. ($t_{air,in,db}$ = 35℃, $t_{air,in,wb}$ = 20℃).

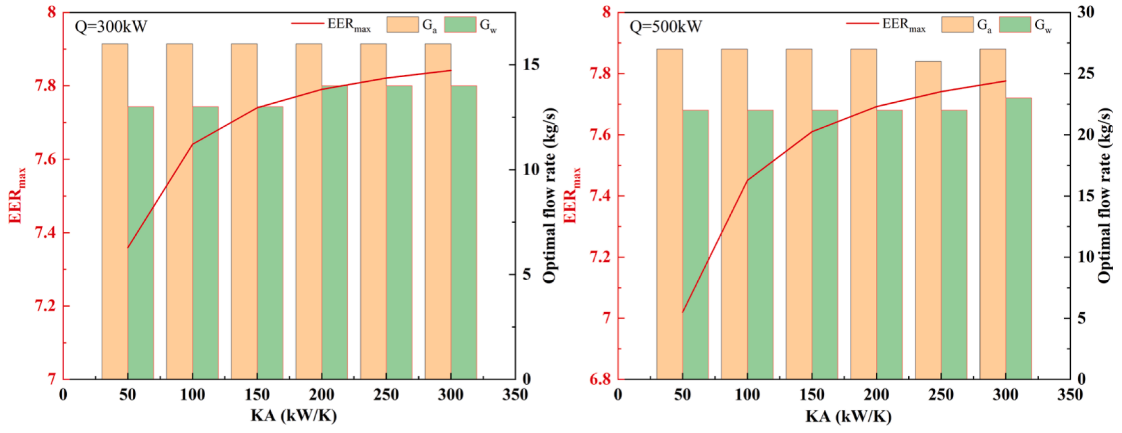

Fig. 10. Optimal flow rate and EER versus heat transfer coefficient. ($t_{air,in,db}$ = 35℃, $t_{air,in,wb}$ = 20℃).

the same inlet air wet-bulb temperature, different relative humidities indicate varying ideal ratios of latent and sensible heat transfer.

Based on the conclusion that the optimal air and water mass flow rate is independent of the padding heat and mass transfer performance and that their ratio is close to 1, engineers can derive the design air and water flow rates combination with the designed cooling capacity, the designed ambient air condition and the designed returning and providing water temperature. The optimal air and water mass flow rate of designed conditions can be approximated by Eq. (43), where Q_s represents the designed cooling capacity, $E_{w,in,s}$ and $t_{w,in,s}$ represent the designed inlet cooling water enthalpy and temperature, and $t_{a,in,wb,s}$ and $E_{a,in,s}$ are the designed operated ambient air enthalpy and temperature, respectively.

$$G_{a,s} \approx \frac{G_{w,s} \cdot c_{pw}\left(t_{w,in,s} - t_{a,in,wb,s}\right)}{\left(E_{w,in,s} - E_{a,in,s}\right)} \approx \frac{Q_s}{\left(E_{w,in,s} - E_{a,in,s}\right)} \tag{43}$$

Eq. (43) is only related to the designed cooling capacity, inlet water temperature, and air wet-bulb temperature. When the padding heat and mass transfer coefficient increase, if the returned cooling water temperature stays the same, the output water temperature decrease and the cooling capacity increase, so that the system EER increase. If the system cooling capacity remains unchanged, the inlet and outlet water temperature will decrease, the COP (coefficient of performance) of the mechanical vapor compression chiller will increase, and the overall EER will also increase. Meanwhile, the optimal *KA* also exists which can minimize the initial investment and life-cycle operating costs of evaporative coolers. The increase in *KA* raises the initial investment but

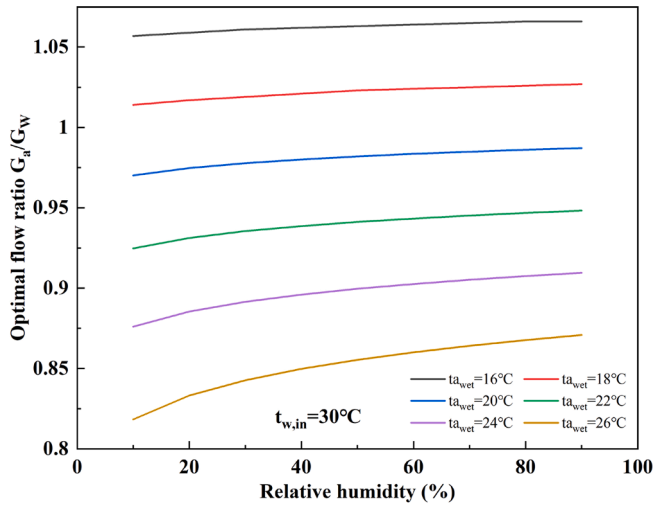

Fig. 11. Ideal optimal flow rate ratio under different inlet air conditions.

improves the COP of vapor compression chillers, which in total keeps the operating costs down.

5.2. Performance comparison of direct and series indirect evaporative cooling

The optimization of air and water flow rates was performed in the previous section, and this section investigates the comparison of DEC and IEC performance with different water allocations of the sensible heat exchanger. This section compares the cooling performance of DEC and series IEC under the same heat and mass transfer coefficient ($KA_{padding}$ = 101 kW/K, KA_{SHE} = 42 kW/K). Series IEC has added sensible heat exchangers compared with DEC, so the water flow rate ratio of SHE is an important parameter for performance comparison. Fig. 12 shows the influence of the water flow rate ratio of SHE and outdoor meteorological conditions. The abscissa indicates the ratio of the flow into the SHE to the total flow into the evaporative cooler. The rest of the flow is sent directly to the top of the padding to be sprayed. Q_{aim} represents the output cooling capacity of evaporative chillers, and Q_{total} is the total heat transfer of SHE and padding. The actual evaporative cooling process under different flow rate ratios is as follows:

(i) Direct evaporative cooling:$G_{w,SHE}/G_w = 0$;
(ii) Indirect evaporative cooling:$0 < G_{w,SHE}/G_w < 100\%$
(iii) Series indirect evaporative cooling:$G_{w,SHE}/G_w = 100\%$

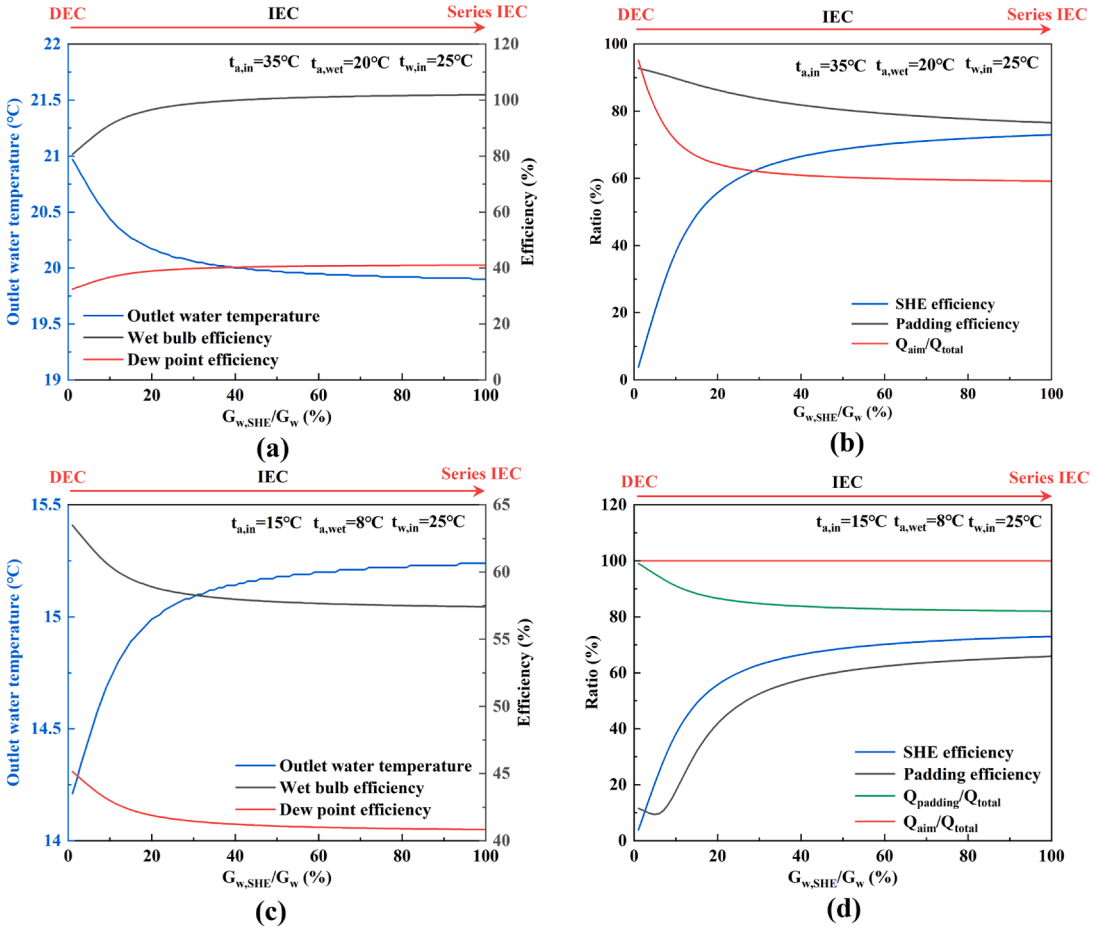

Fig. 12. Effect of the sensible heat exchanger water flow rate ratio and outdoor meteorological conditions; (a) and (c) reflect wet-bulb and dew-point efficiency; (b) and (d) reflect SHE and padding efficiency; (a) and (b): $t_{air,in,db}$ = 35℃, $t_{air,in,wb}$ = 20℃, $t_{water,in}$ = 25℃; (c) and (d): $t_{air,in,db}$ = 15℃, $t_{air,in,wb}$ = 8℃, $t_{water,in}$ = 25℃.

When the inlet air dry-bulb temperature is higher than the inlet water temperature, the wet-bulb and dew-point efficiencies increase with increasing SHE water flow ratio. Series indirect evaporative cooling is the best choice because of its highest wet-bulb and dew-point efficiency. When the inlet air dry-bulb temperature is lower than the inlet water temperature, the opposite results are obtained, in which DEC is the best cooling process.

The SHE efficiency increases and the padding efficiency decreases with increasing $G_{w,SHE}/G_w$, as shown in Fig. 12(b). The series IEC process improves the wet-bulb and dew-point efficiency by increasing the heat transfer of the SHE and padding for higher inlet air dry temperatures. For Fig. 12(c) and (d), both SHE and padding of series IEC reduce the cooling water temperature, and the padding heat transfer decreases, but the overall cooling performance deteriorates. When the sensible heat exchanger cools the inlet air, the air wet-bulb temperature decreases, and the air is closer to the saturation line, which promotes the heat and mass transfer process of padding.

Based on the above analysis, two main effects of the series IEC are demonstrated: the first is that it is possible to have a lower output temperature in hot climates compared to the DEC; and the second is that sensible heat exchangers preheat the inlet ambient air to reduce the freezing risk of padding in cold climates.

To explore the performance differences between DEC and series IEC, the internal temperature and enthalpy distributions are analyzed, as shown in Fig. 13. For series IEC, water and air first transfer heat in the sensible heat exchanger, air temperature drops and water temperature rises. DEC and series IEC have the same process in padding, with air temperature first decreasing and then increasing to produce low-temperature cooling water. However, as a result of the sensible heat exchanger in series IEC, the variation range in air temperature is smaller, and lower water temperature can be obtained than DEC. The air of DEC reaches its minimum temperature at approximately 40% of padding height, while series IEC is approximately 60%.

Fig. 13(b) shows the enthalpy distribution of padding, and the heat and mass transfer process can be regarded as an approximately equal enthalpy difference process. The enthalpy difference of series IEC is approximately 6.8–8.17 kJ/kg, while DEC is only 4.03–4.41 kJ/kg. This indicates that the sensible heat exchanger reduces the air temperature and enlarges the enthalpy difference, which enhances the heat and mass transfer driving force of padding. However, Fig. 12(b) shows that the series indirect evaporative cooling increases the heat transfer capacity of sensible and padding compared with direct evaporative.

According to Fig. 12 and Fig. 13, the series IEC increases the driving force of heat and mass transfer of padding by setting sensible heat exchangers, but also increases the heat transfer capacity. The benefit of increased enthalpy difference is more obvious in dry and hot regions. Series indirect evaporative cooling processes has a better performance in hot and dry climates, and reduces the freezing risk of padding in cold climates.

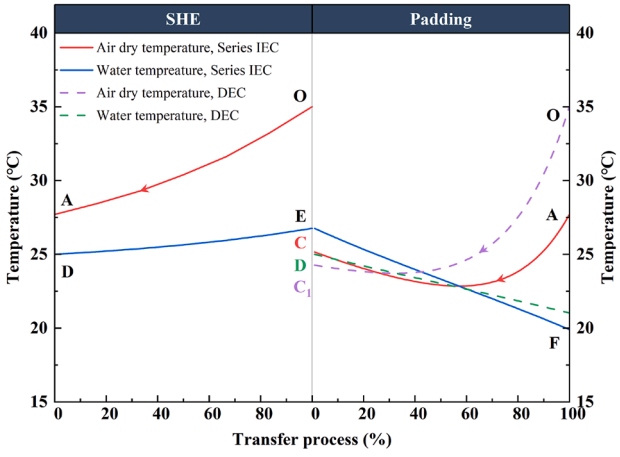

(a) Temperature distribution.

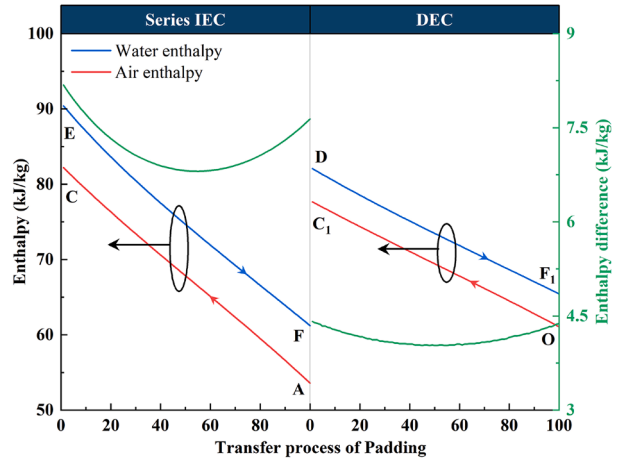

(b) Enthalpy distribution

Fig. 13. Internal distribution of temperature and enthalpy. ($t_{air,in,db}$ = 35℃, $t_{air,in,wb}$ = 20℃, $t_{water,in}$ = 25℃).

5.3. System performance under various climatic conditions

This section compares the DEC and series IEC system performance using the simple traditional case in Fig. 8. For a refrigeration system, different operating modes can be divided according to outdoor climatic conditions, cooling system performance, and cooling water temperature required. Taking Fig. 14(a) as an example, the required cooling water temperature is 10℃, and the designed outlet temperature of cooling water is 16℃. When the output water temperature of DEC is above 16℃, the system must use a vapor compression chiller to produce low-temperature water, and the output water of DEC is used to cool the condenser. The operating mode is known as the vapor compression cooling season. When the DEC output water temperature is 10–16 °C, the output water can provide part of the cooling capacity, which is called transition seasons. When the output temperature of DEC is below 10℃, the system can completely eliminate the use of vapor compression chillers and achieve the full cooling capacity provided by DEC, which is called the free cooling season.

Fig. 14 divides the psychrometric chart into different operating modes according to the system performance. The operating mode can be easily determined from where the outdoor air state is located in the psychrometric chart. The DEC boundary of different operating modes is close to the isenthalpic line, and that of series IEC is between isenthalpic and isothermal. The area of series IEC's transition season and free cooling season is significantly larger than that of DECs. Moreover, series IEC has a larger area in the region of low relative humidity, while DEC has outstanding cooling performance in the high relative humidity region. In humid or cold inlet air conditions, series IEC can improve performance by bypassing the sensible heat exchanger into a direct evaporative cooling process. Another important conclusion found in Fig. 14 is that a higher required cooling water temperature will greatly prolong the duration of the transition season and free cooling season and reduce energy consumption.

DEC performs better in cold and wet climates, while series IEC has good performance in hot and dry climates. The annual meteorological parameters of different regions must be considered to assess system performance. Fig. 15 shows the duration of the free cooling season under different required cooling water temperatures in some cities of DEC, and series IEC refers to meteorological data in 2020. In arid and semiarid

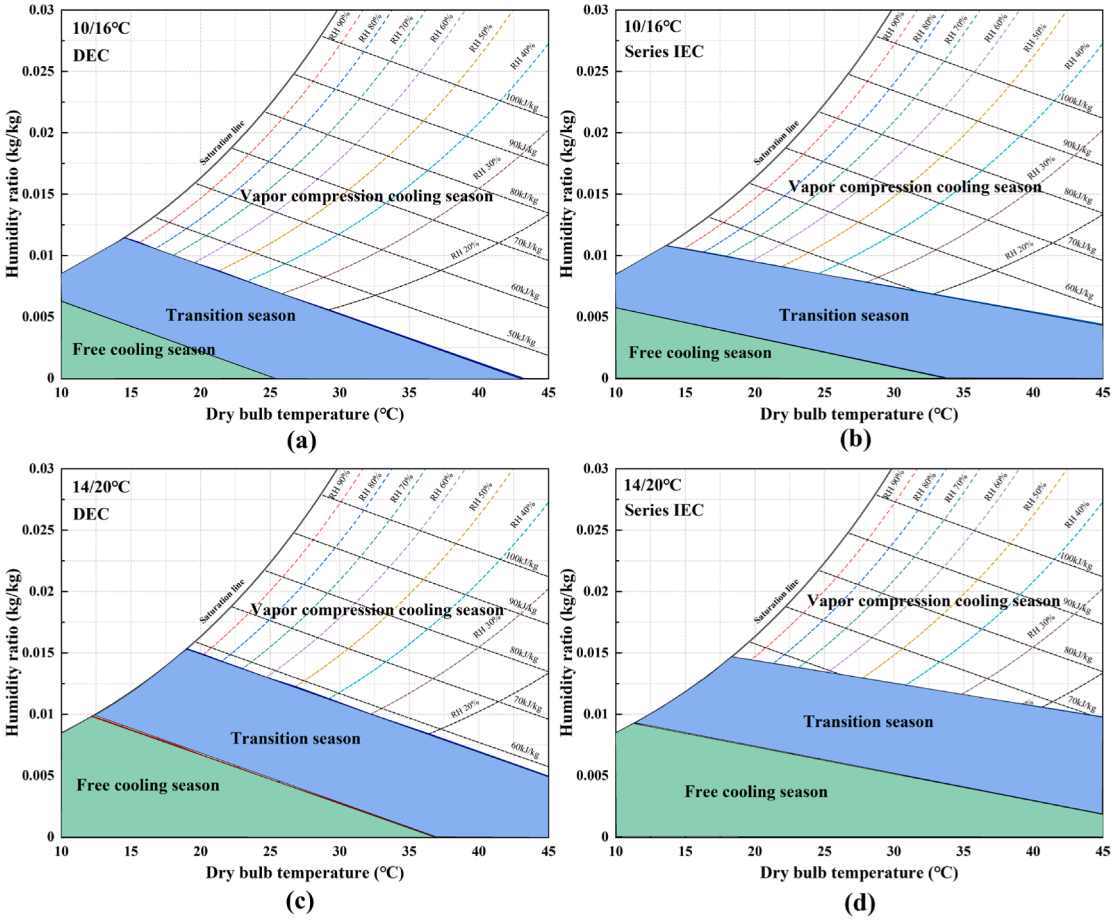

Fig. 14. Operating mode under different supply cooling water temperatures of DEC and series IEC.

regions such as Beijing, Tehran, and Urumqi, series IEC's performance is better than DEC. DEC and series IEC have similar annual cooling performances in Berlin and Canberra. However, in humid regions such as Kunming, Moscow, New York, and London, DEC with better properties could be obtained.

Fig. 14 and Fig. 15 show the meteorological zones and duration for different cooling modes of DEC and series IEC. However, most of the meteorological zones overlap, and the duration of different cooling modes does not differ much. Therefore, the system performance of DEC and series IEC at the same cooling capacity, the same heat and mass transfer coefficient, and the same air and water mass flow rate is compared. The restrictions are as follow:

$$Q_{DEC} = Q_{series} \tag{44}$$

$$t_{w,in,DEC} - t_{w,out,DEC} = t_{w,in,series} - t_{w,out,series} = 5K \tag{45}$$

$$G_{w,DEC} = G_{w,series} = G_{a,DEC} = G_{a,series} \tag{46}$$

where Q_{DEC} and Q_{series} represent the output cooling capacity of DEC and series IEC, and $t_{w,in,DEC}$, $t_{w,out,DEC}$, $t_{w,in,series}$ and $t_{w,out,series}$ are inlet and outlet cooling water temperature of DEC and series IEC. $G_{a,DEC}$, $G_{w,DEC}$, $G_{a,series}$ and $G_{w,series}$ represent and air and water mass flow rate of DEC and series IEC, respectively. The heat transfer coefficients of sensible heat exchangers and padding are 101 kW/K and 42 kW/K.

Fig. 16 shows the results of performance comparison of DEC and series IEC. Under the same conditions of cooling capacity and other equipment parameters, the lower output water temperature leads to better system performance. Thus, Fig. 16 divides the whole psychrometric chart into two parts, with DEC having a lower output water temperature than series IEC in zone 1 and series IEC performing better in zone 2. For different cities' meteorological conditions and system forms, different evaporative cooling can be selected according to the duration in zone 1 and zone 2. It is found that DEC is more suitable for wet and cold regions, while series IEC is more befitting structure in hot and dry regions, as previously concluded.

For example, if a cooling system in Beijing is turned on when the ambient air dry-bulb temperature is greater than 25 ℃, the meteorological parameter points that meet this condition are represented in the psychrometric chart, as shown in Fig. 17. This figure indicates 36.52% of meteorological parameter points fall in zone 1 and 63.48% is located in zone 2, which means that series IEC is more suitable for the system and equipment parameters in Beijing.

There are some limitations in this method of selecting different evaporative cooling structures. The above results do not consider the increase in initial investment in series IEC additional sensible heat exchangers. With the different cooling systems, the operating time of evaporative cooling is different, and the selected meteorological parameter points will also be different. When there is little difference in the proportion of different zones, it is not possible to judge which evaporative cooling is more appropriate in this way. Finally, the division of different evaporative cooling is affected by padding and SHE performance, air flow rate, water flow rate, cooling capacity, etc. Only one example is given in this paper, without considering the influence of these system and equipment parameters.

Freezing direct evaporative cooling systems is a serious operating problem because it takes much labor and energy to solve or prevent, and it thus becomes one of the biggest obstacles to apply DEC in cold regions.

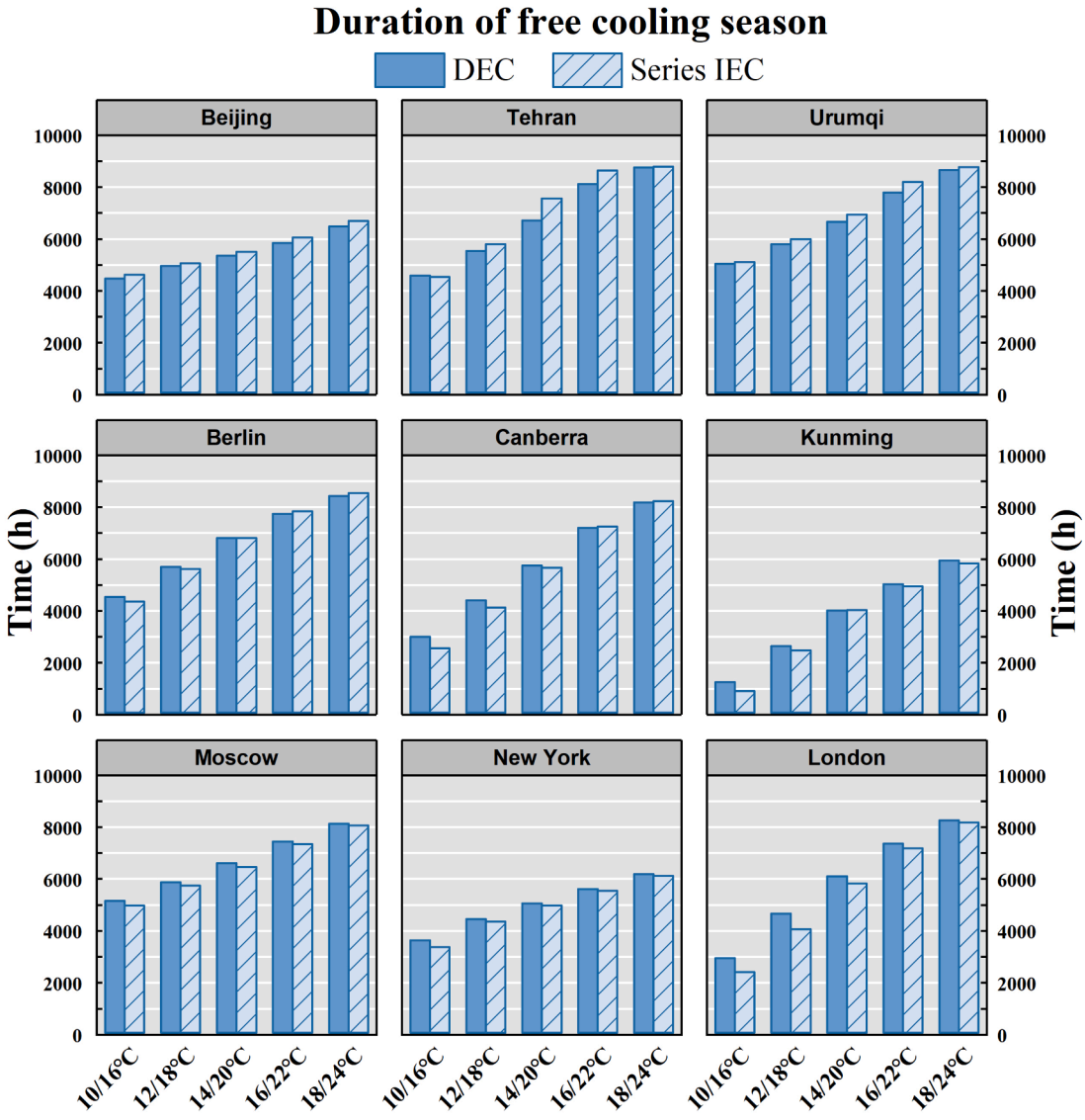

Fig. 15. The duration of the free cooling season versus the required cooling water temperature in different cities.

Closed cooling towers or electric heating protection are usually chosen to prevent this problem, but they perform poorly and consume much energy. For DEC, when cold air first contacts the outermost water of the padding, the heat and mass transfer process of a large air flow rate and small water flow rate has the risk of freezing. Thus, direct evaporative cooling may freeze when the air dry-bulb temperature falls below 0℃. For series IEC, cold air is first heated by inlet water in the sensible heat exchanger, greatly reducing the risk of padding freezing. Water-mediated indirect evaporative chillers actually transfer the freezing risk of padding to SHEs, and the risk can be greatly reduced by setting an appropriate water speed inside SHEs.

Cooling water and ambient air enthalpy difference is large in winter, so it is easy to get required output water temperature. The focus in winter is to prevent the evaporative cooler freeze, when the fan does not work. Thermal pressure ventilation is the most important driving force of the air flow in of evaporative cooling in winter, which is mainly due to the large temperature difference between ambient air and the air inside the evaporative cooler, resulting in the large air density difference. The thermal pressure difference drives the ambient air through sensible heat exchangers and padding to transfer heat and mass with cooling water. The air flow rate is calculated by the following equations:

$$P_h - \Delta P = S \cdot G_a^2 \tag{47}$$

$$P_h \approx g \cdot z \cdot (\rho_a - \rho_{int}) \tag{48}$$

where P_h represents the thermal pressure difference between outlet air and inside air of evaporative coolers.ΔP is resistance and S is the flow coefficient. z represents the height difference of evaporative coolers. ρ_a and ρ_{int} are the densities of air outside and inside the evaporative coolers, respectively.

Fig. 18 shows the freezing risk areas for DEC and series IEC. In series IEC, the water speed in the sensible heat exchanger is set at 1.5 m/s, and the outlet air dry-bulb temperature of the SHE is required to be not less than 10℃. The results show that series IEC is in a freezing risk area only when the inlet air dry-bulb temperature is below −40.88℃. A series IEC achieving no freezing in winter has been developed in Harbin.

A series indirect evaporative cooling process has a better performance in hot or dry climates and is able to bypass SHE to achieve the same cooling effect as the DEC process in cold or wet weather. In addition, series IECs can greatly reduce the risk of freezing, especially in cold regions.

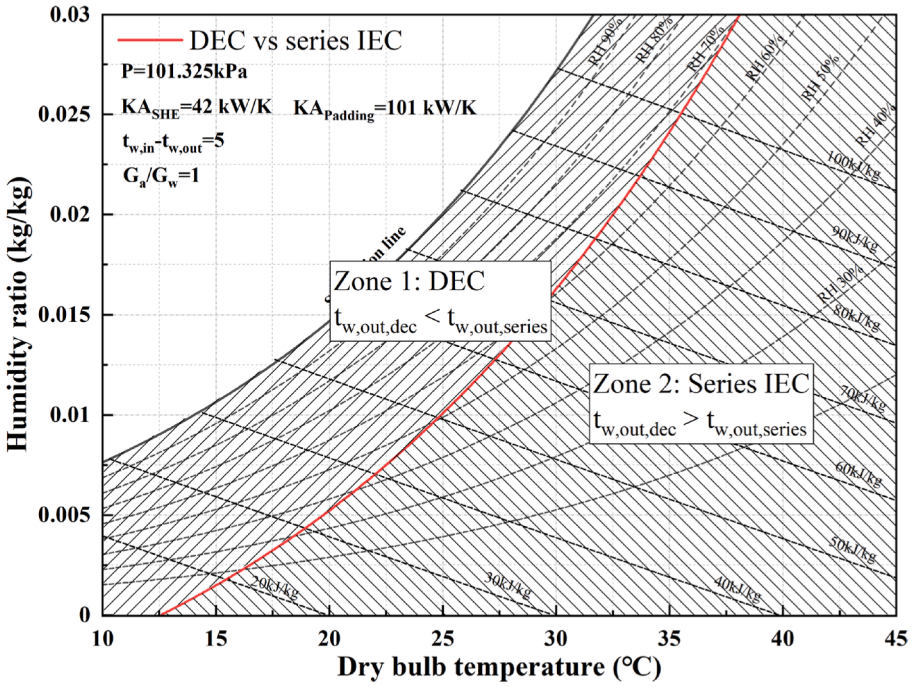

Fig. 16. Performance comparison under different meteorological conditions of DEC and series IEC.

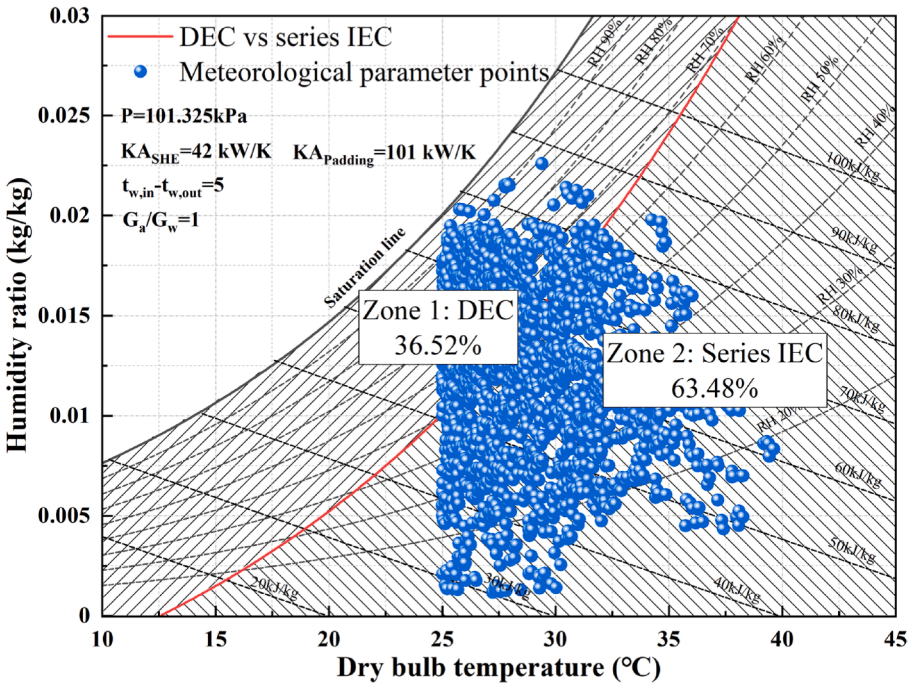

Fig. 17. DEC and series IEC performance under meteorological conditions in Beijing.

6. Conclusion

This paper presents a numerical and experimental investigation of water-mediated series indirect evaporative chillers. The main conclusions are highlighted as follows:

The developed experimental unit can produce cooling water below the air wet-bulb temperature and has a wet-bulb efficiency of over 106.57%, a cooling capacity of 134.28–566.45 kW, a system EER of 3.55–6.31 and a dew-point efficiency of 25.81–53.35% under different operating conditions. The sensible heat coefficient of SHE is calculated to be 30.93 kW/K/m^2, and the heat and mass transfer coefficients are 1.66 kW/K/m^3 and 1.65 kg/s/m^3, respectively.

The simulated model has high accuracy, and the relative error is within 6.61% compared with the experimental results. The air and water flow rates for direct evaporative cooling are optimized by simulation. The optimal air and water flow rates of padding are approximately

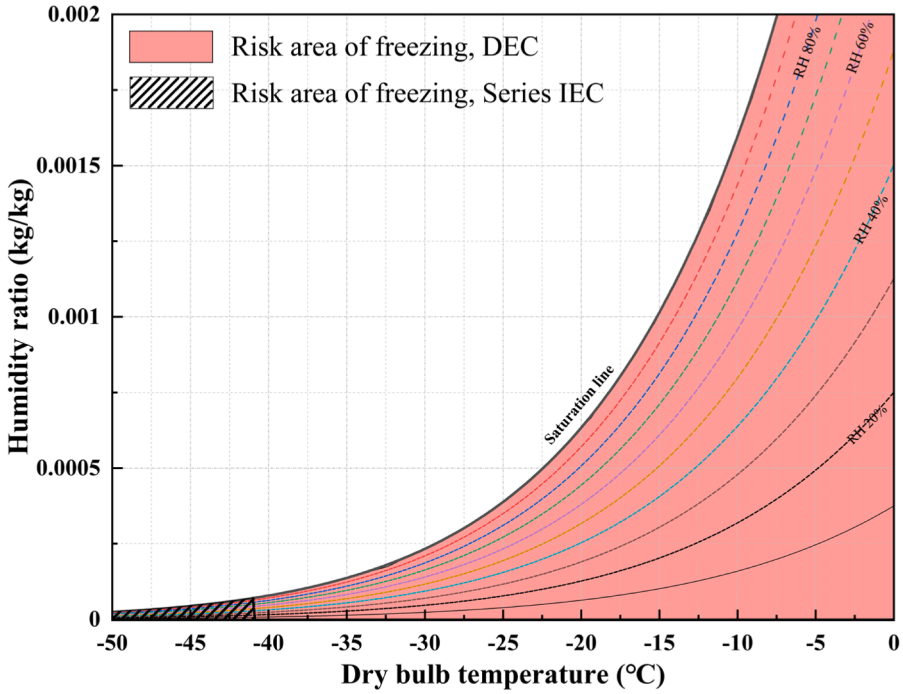

Fig. 18. Comparison of anti-freezing performance.

equal.

The series indirect evaporative cooling process has a better performance in hot and dry regions, while the direct evaporative cooling is more suitable for wet and cold regions. A case study shows that series indirect evaporative cooling is a more befitting process for 63.48% of Beijing's cooling season duration and 36.52% for direct evaporative cooling process. Moreover, series indirect evaporative cooling can greatly reduce the risk of freezing in cold regions, which would not freeze even in the weather of −40.88℃.

Although the present focuses on the experimental and numerical characterizations of the water-mediated series indirect evaporative chiller unit developed for the first time, comparative studies to alternative systems and techno-economic analyses of the investigated system should be performed to comprehensively display the system's potential and advantages in terms of application in hot and dry climate regions as replacement of mechanical vapor compression chillers. Therefore, future studies will focus on essential analysis of the difference between direct and series indirect evaporative cooling and the performance of different water-mediated evaporative cooling technologies in different meteorological parameters and system parameters. Analysis of economy and system performance is helpful to guide engineers to choose the appropriate water-mediated evaporative cooling structure without complex simulation.

CRediT authorship contribution statement

Yang Jing: Conceptualization, Methodology, Software, Validation, Formal analysis, Investigation, Data curation, Resources, Writing – original draft, Writing – review & editing, Visualization. **Ce Zhao:** Validation, Formal analysis, Investigation, Data curation, Resources. **Xiaoyun Xie:** Writing – original draft, Writing – review & editing, Supervision, Project administration, Funding acquisition. **Yi Jiang:** Supervision, Project administration, Funding acquisition.

Declaration of Competing Interest

The authors declare that they have no known competing financial interests or personal relationships that could have appeared to influence the work reported in this paper.

Data availability

Data will be made available on request.

Acknowledgment

The authors gratefully acknowledge the support from National key research and development program of China (key projects of international cooperation in science and technology innovation) (Grant number 2019YFE0102700).

References

[1] World Energy Outlook 2021, IEA. p. 383.
[2] Yang L, Yan H, Lam JC. Thermal comfort and building energy consumption implications – A review. Appl Energy 2014;115:164–73.
[3] Pérez-Lombard L, Ortiz J, Pout C. A review on buildings energy consumption information. Energy Build 2008;40(3):394–8.
[4] 2020 ASHRAE Handbook - HVAC Systems and Equipment (SI Edition). 2020: American Society of Heating Refrigerating and Air-Conditioning Engineers Inc. ASHRAE.
[5] Cui X, Chua KJ, Islam MR, Ng KC. Performance evaluation of an indirect pre-cooling evaporative heat exchanger operating in hot and humid climate. Energy Convers Manage 2015;102:140–50.
[6] Delfani S, Esmaeelian J, Pasdarshahri H, Karami M. Energy saving potential of an indirect evaporative cooler as a pre-cooling unit for mechanical cooling systems in Iran. Energy Build 2010;42(11):2169–76.
[7] Porumb B, Bălan M, Porumb R. Potential of Indirect Evaporative Cooling to Reduce the Energy Consumption in Fresh Air Conditioning Applications. Energy Procedia 2016;85:433–41.
[8] Heidarinejad G, Bozorgmehr M, Delfani S, Esmaeelian J. Experimental investigation of two-stage indirect/direct evaporative cooling system in various climatic conditions. Build Environ 2009;44(10):2073–9.
[9] Fikri B, Sofia E, Putra N. Experimental analysis of a multistage direct-indirect evaporative cooler using a straight heat pipe. Appl Therm Eng 2020;171:115133.

[10] Yang Y, Cui G, Lan CQ. Developments in evaporative cooling and enhanced evaporative cooling - A review. Renew Sustain Energy Rev 2019;113:109230.
[11] Alam MF, et al. An experimental study on the design, performance and suitability of evaporative cooling system using different indigenous materials. AIP Conf Proc 2017;1851(1).
[12] Al-Sulaiman F. Evaluation of the performance of local fibers in evaporative cooling. Energy Convers Manage 2002;43(16):2267–73.
[13] Bishoyi D, Sudhakar K. Experimental performance of a direct evaporative cooler in composite climate of India. Energy Build 2017;153:190–200.
[14] Pu S, Fu J, Liao Y, Ge L, Zhou Y, Zhang S, et al. Promoting Energy Efficiency via a Self-Adaptive Evaporative Cooling Hydrogel. Adv Mater 2020;32(17):1907307.
[15] Liao C, Chiu K. Wind tunnel modeling the system performance of alternative evaporative cooling pads in Taiwan region. Build Environ 2002;37(2):177–87.
[16] Min Y, et al. Enhancing the cooling and dehumidification performance of indirect evaporative cooler by hydrophobic-coated primary air channels. Int J Heat Mass Transf 2021;179:121733.
[17] Kashyap S, Sarkar J, Kumar A. Exergy, economic, environmental and sustainability analyses of possible regenerative evaporative cooling device topologies. Build Environ 2020;180:107033.
[18] Kashif M, Niaz H, Sultan M, Miyazaki T, Feng Y, Usman M, et al. Study on Desiccant and Evaporative Cooling Systems for Livestock Thermal Comfort: Theory and Experiments. Energies 2020;13(11):2675.
[19] Shirmohammadi R, Gilani N. Effectiveness Enhancement and Performance Evaluation of Indirect-Direct Evaporative Cooling System for a wide Variety of Climates. Sustainable. Energy 2019;38(3):e13032.
[20] Sohani A, Sayyaadi H, Azimi M. Employing static and dynamic optimization approaches on a desiccant-enhanced indirect evaporative cooling system. Energy Convers Manage 2019;199:112017.
[21] Harrouz JP, Ghali K, Ghaddar N. Integrated solar – Windcatcher with dew-point indirect evaporative cooler for classrooms. Appl Therm Eng 2021;188:116654.
[22] Zhao R, Liu J, Gu J, Zhai L, Ma F. Experimental study of a direct evaporative cooling approach for Li-ion battery thermal management. Int J Energy Res 2020;44 (8):6660–73.
[23] Al Horr Y, et al. Operational mode optimization of indirect evaporative cooling in hot climates. Case Stud Therm Eng 2020;18:100574.
[24] Pandelidis D, et al. Performance study of a novel dew point evaporative cooler in the climate of central Europe using building simulation tools. Build Environ 2020; 181:107101.
[25] Xuan YM, Xiao F, Niu XF, Huang X, Wang SW. Research and applications of evaporative cooling in China: A review (II)—Systems and equipment. Renew Sustain Energy Rev 2012;16(5):3523–34.
[26] Sibanda S, Workneh TS. Performance evaluation of an indirect air cooling system combined with evaporative cooling. Heliyon 2020;6(1). p. e03286.
[27] La D, Dai YJ, Li Y, Tang ZY, Ge TS, Wang RZ. An experimental investigation on the integration of two-stage dehumidification and regenerative evaporative cooling. Appl Energy 2013;102:1218–28.
[28] Jiang Y, Xie X. Theoretical and testing performance of an innovative indirect evaporative chiller. Sol Energy 2010;84(12):2041–55.
[29] Xiaoyun X, Yi J. Thermological principle of moist air heat and moisture conversion processes. J HV&AC 2011;41(03). p. 65-76+21.
[30] De Antonellis S, Joppolo CM, Liberati P, Milani S, Romano F. Modeling and experimental study of an indirect evaporative cooler. Energy Build 2017;142: 147–57.
[31] Zheng B, et al. Development of an experimental validated model of cross-flow indirect evaporative cooler with condensation. Appl Energy 2019;252:113438.
[32] Matsui K, Thu K, Miyazaki T. A hybrid power cycle using an inverted Brayton cycle with an indirect evaporative device for waste-heat recovery. Appl Therm Eng 2020; 170:115029.